Inorg. Chem. **2009**, *48*, 3710−3719

Polynuclear Spin Crossover Complexes: Synthesis, Structure, and Magnetic Behavior of $[Fe_4(\mu\text{-}CN)_4(phen)_4(L)_2)]^{4+}$ Squares

Ishtvan Boldog,[†] Francisco J. Muñoz-Lara,[†] Ana B. Gaspar,[†] M. Carmen Muñoz,[‡] Maksym Seredyuk,[§] and José A. Real*,[†]

Institut de Ciència Molecular (ICMol)/Departament de Química Inorgànica, Universitat de València, Edifici de Instituts de Paterna, P.O. Box 22085, 46071, València, Spain, Departament de Física Aplicada, Universitat Politècnica de València, Camí de Vera s/n, 46022, València, Spain, and Institut für Anorganische and Analystiche Chemie, Johannes-Gutenberg-Universität, Staudinger-Weg 9, D-55099 Mainz, Germany

Received December 2, 2008

Three new tetranuclear compounds of formula $[Fe_4(\mu\text{-}CN)_4(phen)_4(L)_2)](PF_6)_4 \cdot G$ where L = tris(pyridin-2-ylmethyl)amine (TPMA) [G = 0] (**1**), (6-methylpyrid-2-ylmethyl)-bis(pyrid-2-ylmethyl)amine (MeTPMA) [G = 0] (**2**), or bis(6-methylpyrid-2-ylmethyl)-(pyrid-2-ylmethyl)amine (Me_2TPMA) [G = NH_4PF_6] (**3**) and phen = 1,10-phenanthroline) have been synthesized and characterized. The three compounds crystallize in the *C*2/*c* space group and consist of $[Fe_4(\mu\text{-}CN)_4(phen)_4(L)_2)]^{4+}$ square shaped cations with two distinct iron(II) sites. The sites, associated with $[Fe(phen)_2(CN)_2]$ and $[Fe(L)(NC)_2]$ moieties, are connected by cyanide bridging ligands and reside in different $[FeN_4C_2]$ and $[FeN_6]$ ligand field strength environments. For **1**, the structural features of both sites at 100 and 293 K are those of an iron(II) atom in the low-spin state, according to the magnetic properties. At 370 K the structure of the $[FeN_6]$ site is consistent with a quite complete change of spin state from the low-spin state to the high-spin state, a behavior confirmed by the magnetic study. Introduction of a methyl substituent in the sixth position of one or two pyridine groups to get MeTPMA or Me_2TPMA derivatives, respectively, induce in **2** and **3** notable steric constraint in the $[FeN_6]$ site making longer the average Fe−N bond distances thereby weakening the ligand field strength and stabilizing the high-spin state. The $[FeN_4C_2]$ site remains in the low-spin state in the three compounds.

Introduction

Strong interest is currently devoted to switchable molecular materials made up of iron(II) spin crossover (SCO) building blocks exhibiting cooperative behavior since they can manifest sensory and memory functions. A transfer of two electrons between the e_g and t_{2g} orbitals and a synchronous change of size, by about 25%, of the iron(II) ion is the origin of such a cooperative response to external stimuli like temperature, pressure, and light irradiation.[1] In mononuclear compounds cooperativity stems from efficient intermolecular interactions (i.e., strong hydrogen bonds and/or π-π interactions). In coordination 1D−3D polymers, cooperativity essentially originates from efficient interactions between iron(II) centers through rigid bridging ligands.[2] Between both categories of compounds, discrete polynuclear iron(II) SCO complexes represent a class of molecular materials with potential interesting SCO properties at the molecular nanodomain scale. In this respect, a relatively large number of dinuclear iron(II) complexes have been synthesized,[3] among them those derived from the generic family {[Fe(L)-

* To whom correspondence should be addressed. E-mail: jose.a.real@uv.es.
[†] Universitat de València.
[‡] Universitat Politècnica de València.
[§] Johannes-Gutenberg-Universität.

(1) (a) Real, J. A.; Gaspar, A. B.; Muñoz, M. C. *Dalton Trans.* **2005**, 2062. (b) Gaspar, A. B.; Ksenofontov, V.; Seredyuk, M.; Gütlich, P. *Coord. Chem. Rev.* **2005**, *249*, 2661. (c) Spin Crossover in Transition Metal Compounds. In *Topics in Current Chemistry*; Gütlich, P., Goodwin, H. A., Eds.; Springer: New York, 2004; pp 233−235. (d) Gütlich, P.; Hauser, A.; Spiering, H. *Angew. Chem., Int. Ed. Engl.* **1994**, *33*, 2024. (e) König, E. *Struct. Bonding (Berlin)* **1991**, *76*, 51. (f) Gütlich, P. *Struct. Bonding (Berlin)* **1981**, *44*, 83. (g) Goodwin, H. A. *Coord. Chem. Rev.* **1976**, *18*, 293.

(2) (a) García, Y.; Niel, V.; Muñoz, M. C.; Real, J. A. *Top. Curr. Chem.* **2003**, *233*, 229. (b) Real, J. A.; Gaspar, A. B.; Niel, V.; Muñoz, M. C. *Coord. Chem. Rev.* **2003**, *235*, 121.

(3) Gaspar, A. B.; Muñoz, M. C.; Real, J. A. *J. Mater. Chem.* **2006**, *16*, 2522; and references therein.

10.1021/ic802306r CCC: $40.75
Published on Web 03/13/2009

$(NCX)_2]_2$bpym} (L = α-diimine, X = S, Se) have been studied in depth. In particular it has been shown that the derivatives {[Fe(bpym)$(NCX)_2]_2$bpym} and {[Fe(bt)$(NCX)_2]_2$-bpym} (bt = 2,2′-bithiazoline) undergo two-step thermally induced spin transition (at different pressures) and light-induced transitions as well.[4] The two steps reflect the occurrence of three spin-pair states (quintet-quintet, singlet-quintet, and singlet−singlet) which have been monitored using Mössbauer spectroscopy in the presence of intense magnetic fields. The singlet-quintet state corresponds to the plateau between the two steps. More recently, selective transformation between these states was achieved by irradiating the complex with red and infrared light of appropriate wavelength and monitored using Raman spectroscopy and single-crystal X-ray data.[5] These results can be considered a first step in the search for multiswitchable polynuclear SCO molecules of nanometric dimensions.

A natural extension of this work requires the synthesis of polynuclear complexes with three or more SCO iron(II) ions. This is an almost unexplored field most probably because of inherent difficulties to synthesize appropriate multidentate ligands or metallo-ligands able to provide the appropriate ligand field strength at the iron(II). Indeed, up to date, only two classes of tetranuclear iron(II) systems have been reported. One, synthesized by Lehn et al., corresponds to $[Fe_4L_4](X)_8$ (L is 4,6-bis(2′,2″-bipyrid-6′-yl)-2-phenyl-pyrimidine or derivatives of this ligand; X = ClO_4^-, PF_6^-, BF_4^-) and represents a [2 × 2]-like cationic grid system which undergoes a continuous incomplete spin transition.[6] The second class corresponds to a cyanide-bridged ferrous tetranuclear square-complexes with formula $[Fe_4(\mu\text{-}CN)_4(2,2'\text{-bipy})_4(TPMA)_2)](X)_4$ (2,2′-bipy = 2,2′-bipyridine; TPMA = tris(pyridin-2-ylmethyl)amine; X = BF_4^-, PF_6^-). In this complex there are two different sites; one, [Fe(2,2′-$bipy)_2(NC)_2$], is low-spin whereas the other, [Fe(TPMA)-$(CN)_2$], exhibits SCO. Oshio et al. have demonstrated that the two SCO iron sites undergo spin transition at different characteristic temperatures ($T_{1/2}(1)$ = 160 K and $T_{1/2}(2)$ > 350 K) for the PF_6^- salt.[7] The BF_4^- derivative was previously synthesized by Vahrenkamp et al.,[8] and the structural information indicates that it may display a similar magnetic behavior. Aside from tetranuclear complexes, more recently Dunbar, Achim, and co-workers have reported the syntheses of $\{[Fe(tmphen)_2]_3[M^{III}(CN)_6]_2\}$ (M^{III} = Fe, Co, tmphen is 3,4,7,8-tetramethyl-1,10-phenanthroline) pentanuclear cyanide clusters in which the three iron(II) moieties display continuous SCO behavior.[9]

Chart 1

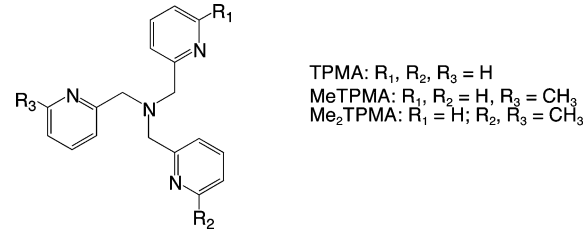

Here we report the synthesis, crystal structures, and magnetic properties of the new iron(II) square complexes $[Fe_4(\mu\text{-}CN)_4(phen)_4(L)_2)](PF_6)_4 \cdot G$ by using a series of tetradentate ligands L (see Chart 1) able to generate varied ligand field strength: tris(pyridin-2-ylmethyl)amine (TPMA) [G = 0] (**1**), 6-methylpyrid-2-ylmethyl)-bis(pyrid-2-ylmethyl)amine (MeTPMA) [G = 0] (**2**), and bis(6-methylpyrid-2-ylmethyl)-(pyrid-2-ylmethyl)amine (Me_2TPMA) [G = NH_4PF_6] (**3**) (phen is 1,10-phenanthroline).

Materials and Methods

All chemicals and solvents used were of commercial grade and used without further purification with the exception of solvents specified below. Methanol was deoxygenated by distillation under argon, acetonitrile and ether for specified repeated experiments were distilled under argon over CaH_2 and sodium diphenylketyl, respectively. 6-Methylpyrid-2-ylamine and dicyanobis(2,2′-phenanthroline)iron(II) dihydrate, $(Fe(phen)_2(CN)_2 \cdot 2H_2O)$,[10] were prepared by literature methods (the cyanocomplex of iron was not stored for a long time because of deterioration). All operations with the Fe(II) containing solutions were performed under argon atmosphere; short air contact was not found to be detrimental for the solutions of the reported polynuclear complexes, but prolonged exposures yielded Fe(III) compounds also.

Syntheses of the Ligands. The ligands TPMA, MeTPMA, and Me_2TPMA were synthesized according to the literature method described before for the synthesis of tris(6-methyl-2-pyridylmethylamine).[11]

Me_2TPMA. A CH_2Cl_2 solution (50 mL) of 6-methylpyrid-2-ylmethylbromide (37.6 mmol, 7 g) was added dropwise to a water solution (60 mL) of pyrid-2-ylmethylamine (18.8 mmol, 2 g) cooled at 0 °C. After stirring for 15 min, 1.51 g (37.6 mmol) of NaOH were added, and the red biphasic solution was left to stir for 3 days. The organic layer was separated then, and the aqueous phase was extracted with CH_2Cl_2 (3 × 30 mL). The combined organic extracts were dried with anhydrous Na_2SO_4, filtered, and the filtrate was rotary-evaporated to give a brown oil, which is solidified

(4) (a) Real, J. A.; Gaspar, A. B.; Muñoz, M. C.; Gütlich, P.; Ksenofontov, V.; Spiering, H. *Top. Curr. Chem.* **2004**, *233*, 167. (b) Bousseksou, A.; Molnár, G.; Real, J. A.; Tanaka, K. *Coord. Chem. Rev.* **2007**, *251*, 1822.

(5) (a) Ould Moussa, N.; Molnár, G.; Bonhommeau, S.; Zwick, A.; Mouri, S.; Tanaka, K.; Real, J. A.; Bousseksou, A. *Phys. Rev. Lett.* **2005**, *94*, 107245. (b) Ould Moussa, N.; Trzop, E.; Mouri, S.; Zein, S.; Molnár, G.; Gaspar, A. B.; Collet, E.; Buron-Le Cointe, M.; Real, J. A.; Borshch, S. A.; Tanaka, K.; Cailleau, H.; Bousseksou, A. *Phys. Rev. B* **2007**, *75*, 054101. (c) Trzop, E.; Buron-Le Cointe, M.; Cailleau, H.; Toupet, L.; Molnár, G.; Bousseksou, A.; Gaspar, A. B.; Real, J. A.; Collet, E. *J. Appl. Crystallogr.* **2007**, *40*, 158. (d) Gaspar, A. B.; Ksenofontov, V.; Reiman, S.; Gütlich, P.; Thompson, A. L.; Goeta, A. E.; Muñoz, M. C.; Real, J. A. *Chem.—Eur. J.* **2006**, *12*, 9289.

(6) (a) Breuning, E.; Ruben, M.; Lehn, J. M.; Renz, F.; Garcia, Y.; Ksenofontov, V.; Gütlich, P.; Wegelius, E.; Rissanen, K. *Angew. Chem., Int. Ed.* **2000**, *39*, 2504. (b) Ruben, M.; Breuning, E.; Lehn, J. M.; Ksenofontov, V.; Renz, F.; Gütlich, P.; Vaughan, G. B. M. *Chem.—Eur. J.* **2003**, *9*, 4422. (c) Alam, M. S.; Strömsdörfer, S.; Dremov, V.; Müller, P.; Kortus, J.; Ruben, M.; Lehn, J. M. *Angew. Chem., Int. Ed.* **2005**, *44*, 7896. (d) Ruben, M.; Ziener, U.; Lehn, J. M.; Ksenofontov, V.; Gütlich, P.; Vaughan, G. B. M. *Chem.—Eur. J.* **2005**, *11*, 94.

(7) Nihei, M.; Ui, M.; Yokota, M.; Han, L.; Maeda, A.; Kishida, H.; Okamoto, H.; Oshio, H. *Angew. Chem., Int. Ed.* **2005**, *44*, 6487.

(8) Flay, M. L.; Compte, V.; Vahrenkamp, H. *Z. Anorg. Allg. Chem.* **2003**, *629*, 1147.

(9) Shatruk, M.; Dragulescu-Andrasi, A.; Chambers, K. E.; Stolan, S. A.; Bominaar, C.; Achim, E. L.; Dunbar, K. R. *J. Am. Chem. Soc.* **2007**, *129*, 6104.

(10) Schilt, A. A. *Inorg. Synth.* **1970**, *XII*, 247.

(11) Gultneh, Y.; Yisgedu, T. B.; Tesema, Y. T.; Butcher, R. J. *Inorg. Chem.* **2003**, *42*, 1857.

immediately upon cooling. The product was purified further by flash-chromatography (MeOH: EtOAc: Et_3N = 10:90:2, v/v) to give 4.2 g (70%) of slightly yellow product. NMR δ_H (300 MHz, $CDCl_3$, T = 20 °C) 2.52 (6H, s, CH_3), 3.89 (6H, s, CH_2(Mepy)), 3.91 (3H, s, CH_2(py)), 7.00 (2H, d, $J_{MepyH4,\ MepyH5}$ = 7.5, MepyH5), 7.13 (1H, dd, $J_{pyH4pyH5} \sim 6.9$, $J_{pyH5pyH6}$ = 4.8), 7.43 (2H, d, $J_{MepyH3,\ MepyH4}$ = 7.8, MepyH3), 7.55 (2H, dd, $J_{MepyH3,\ MepyH4}$ = 7.8, $J_{MepyH4,\ MepyH5}$ = 7.5, MepyH4), 7.60 (1H, d, $J_{pyH3,\ pyH4}$ = 7.5 pyH3), 7.65 (1H, dd, $J_{pyH3,\ pyH4}$ = 7.5, $J_{pyH4,\ pyH5}$ = 6.9, pyH4), 8.52 (1H, d, $J_{pyH5,\ pyH6}$ = 4.8, pyH6). The obtained data is consistent with that reported in the literature.[12]

TPMA and **MeTPMA** were synthesized following an identical procedure, starting from 2-bromomethylpyridine hydrobromide, 2-pyridylamine, or 6-methylpyrid-2-yl amine, respectively, and double amount of base. TPMA was purified by recrystallization from petroleum ether/CH_2Cl_2 4:1 mixture that yielded the product as a light yellow solid (65%). NMR δ_H (300 MHz, $CDCl_3$, T = 20 °C) 3.97 (6H, s, CH_2), 7.16 (3H, dd, $J_{pyH5,\ pyH6}$ = 4.8, $J_{pyH4,\ pyH5} \sim 8$, pyH5), 7.59 (3H, d, $J_{pyH3,\ pyH4}$ = 7.8, pyH3), 7.67 (3H, dd, $J_{pyH3,\ pyH4} \sim 7.8$, $J_{pyH4,\ pyH5} \sim 8$, pyH4), 8.54 (3H, d, $J_{pyH5,\ pyH6}$ = 4.8, pyH6) is consistent with the values given in the literature.[13] MeTPMA was purified as described for Me_2TPMA (the yield of the light yellow solid was 46%). NMR (δ_H (300 MHz, $CDCl_3$, T = 20 °C) 2.53 (3H, s, CH_3), 3.86 (2H, s, CH_2(MePy)), 3.89 (4H, s, CH_2(py)), 7.00 (1H, d, $J_{MepyH4,\ MepyH5}$ = 7.5, MepyH5); 7.14 (2H, dd, $J_{pyH4,\ pyH5}$ = 7.2, $J_{pyH5,\ pyH6}$ = 4.8, pyH5), 7.43 (1H, d, $J_{MepyH3,\ MepyH4}$ = 7.8, MepyH4), 7.55 (1H, dd, $J_{MepyH3,\ MepyH4}$ = 7.8, $J_{MepyH4,\ MepyH5}$ = 7.5, MepyH4), 7.60 (2H, d, $J_{pyH3,\ pyH4}$ = 7.8, pyH3), 7.66 (2H, dd, $J_{pyH3,\ pyH4}$ = 7.8, $J_{pyH4,\ pyH5}$ = 7.2, pyH4), 8.53 (2H, dd, $J_{pyH5,\ pyH6}$ = 4.8, pyH6). These values are consistent with those given in the literature.[12]

The employed method was proven to be more convenient for the synthesis of the ligand in comparison with the known one pot reduction of 2-pyridinecarboxaldehyde and 2-aminomethylpyridine by sodium triacetoxyborohydride.[12,13] The second method allowed us to achieve 69% max. yield, but the yields in other repeated experiments were generally lower.

Synthesis of Coordination Compounds. The synthetic procedure for obtaining **1**−**3** was similar for the three compounds. The synthesis of $[Fe_4(CN)_4(phen)_4(MeTPMA)_2](PF_6)_4$ (**2**) is described in detail as an example. A 165 mg quantity (0.33 mmol) of $Fe(CN)_2(phen)_2 \cdot 2H_2O$ was dissolved in 60 mL of deoxygenated MeOH, and the formed solution was filtered to remove some minor residues. A second solution, containing 65 mg (0.33 mmol) of $FeCl_2 \cdot 4H_2O$ and 100 mg (0.33 mmol) of MeTPMA in 10 mL of MeOH was prepared and left stirring for 15 min. This solution was poured into the first during 5 min, and the formed clear solution was left stirring for 1 day. A 215 mg quantity (1.32 mmol, ×2 excess) of NH_4PF_6 in 40 mL of MeOH was added dropwise under stirring during 15 min, accompanied with gradual precipitation of the product. After 4 h of stirring, the precipitate was filtered off and dried under argon. The obtained product contained minor impurities including NH_4PF_6, which were mostly removed before recrystallization by dissolving the product in minimal amount of acetonitrile and centrifuging off the gray insoluble precipitate. Yield of **2** in a form of the dark red microcrystalline solid was 87%. IR (KBr), ν_{max}/cm^{-1}: 3650w, 3424m, 3087w, 2921w, 2096s shoulder (CN), 1604m, 1575w, 1429m, 1414w, 840s (PF_6), 771w, 725m, 557m. Anal. Calcd (Found) (%) for $C_{90}H_{72}N_{20}F_{24}Fe_4P_4$ (**2**) (red): C 48.32 (48.10), H 3.24 (3.18), N 12.52 (12.33). **1**, deep-red microcrystalline solid, yield 69%. Freshly isolated crystals correspond to **1**·CH_3CN·H_2O solvate according to single crystal X-ray diffraction structure determination at low temperatures (see below), but on drying or even exposure to open air it loses solvent and converts to **1**. IR (KBr), ν_{max}/cm^{-1}: 3660w, 3434m, 3082w, 2925w, 2090s, 1639w, 1604m, 1479s, 1444w, 1429m, 1413w, 841s (PF_6), 768m, 723m, 557m. Anal. Calcd (Found) (%) for $C_{88}H_{68}N_{20}F_{24}Fe_4P_4$ (**1**) (red): C 47.85 (47.46), H 3.10 (3.03), N 12.68 (12.46).

3, red microcrystalline solid, yield 83%. IR (KBr), ν_{max}/cm^{-1}: 3651w, 3434m, 3087w, 2925w, 2092s (CN), 1630w, 1604m, 1577w, 1468w, 1454 w, 1429m, 1414w, 840s (PF_6), 725m, 557m. Anal. Calcd (Found) (%) for $C_{92}H_{80}N_{21}F_{30}Fe_4P_5$ (**3**) (red): C 45.51 (45.11), H 3.32 (3.,22), N 12.11 (11.98).

Crystals suitable for single crystal X-ray diffraction (XRD) were grown by vapor diffusion of diethyl ether in a about 15 mg/mL solution of **1**−**3** in acetonitrile.

X-ray Crystallography. Diffraction data on crystals of **1/1**·CH_3CN·H_2O were collected at 100, 293, and 370 K while for **2** and **3** they were collected at 293 and 160 K, respectively, using a Nonius Kappa-CCD single crystal diffractometer using graphite monochromated Mo Kα radiation (λ = 0.71073 Å). A multiscan absorption correction was performed but not applied. The absorption correction was found to have no significant effect on the refinement results. The structures were solved by direct methods using SHELXS-97 and refined by full-matrix least-squares on F^2 using SHELXL-97.[14] All non-hydrogen atoms were refined anisotropically except for **1** at 293 and 370 K where the nitrogen and carbon atoms were refined isotropically. Relevant crystallographic data are displayed in Table 1.

Magnetic Susceptibility Measurements. The variable-temperature magnetic susceptibility measurements were carried out between 4 and 400 K using a Quantum Design MPMS2 SQUID magnetometer operating at 1 T magnetic field. The susceptometer was calibrated with $(NH_4)_2Mn(SO_4)_2 \cdot 12H_2O$. The independence of the susceptibility with regard to the applied magnetic field was checked at room temperature for each compound. The temperature was varied at a rate of 1 K min^{-1} in the heating and cooling modes. Experimental susceptibilities were corrected for diamagnetism of the constituent atoms by the use of Pascal's constants.

^{57}Fe Mössbauer Spectroscopy. Mössbauer measurements on **3** were carried out in a flow-type liquid nitrogen cryostat using a conventional constant acceleration type Mössbauer spectrometer; γ-rays were provided by a ^{57}Co(Rh) source (50 mCi). The spectrum evaluations were done with the assumption of Lorentzian line shapes using the Recoil software.[15] All isomer shifts are given relative to α-Fe at room temperature.

Results

Crystal Structure of 1. The crystal structure of **1** was determined at 100, 293, and 370 K. A single crystal isolated from the mother solution was mounted on the goniometric head and cooled immediately to 100 K. The single crystal analysis at 100 K revealed the occurrence of two labile solvent molecules: one molecule of acetonitrile and one molecule of water (**1**·CH_3CN·H_2O). Both solvent molecules were easily removed in a single crystal-to-single crystal transformation when temperature was raised up to 293 K.

(12) Nagao, H.; Komeda, N.; Mukaida, M.; Suzuki, M.; Tanaka, K. *Inorg. Chem.* **1996**, *35*, 6809.
(13) Jenkins, H. A.; Klempner, M. J.; Prokopchuk, E. M.; Puddephatt, R. J. *Inorg. Chim. Acta* **2003**, *352*, 72.
(14) Sheldrick, G. M. *SHELX97: Program for Crystal Structure Determination*; University of Göttingen: Göttingen, Germany, 1997.
(15) http://www.isapps.ca/recoil/.

Table 1. Crystal Data for **1**, **2**, and **3**

	1			**2**	**3**
	370 K	293 K	100 K	293 K	160 K
empirical formula	$C_{88}H_{68}N_{20}P_4F_{24}Fe_4$		$C_{90}H_{73}N_{21}O_1P_4F_{24}Fe_4$	$C_{90}H_{72}N_{20}P_4F_{24}Fe_4$	$C_{92}H_{76}N_{20}P_5F_{30}Fe_4$
M_r	2208.90		2267.97	2236.96	2409.98
crystal system	monoclinic			monoclinic	monoclinic
space group	*C*2/*c*			*C*2/*c*	*C*2/*c*
a (Å)	28.5230(5)	28.4440(13)	28.2470(7)	29.1810(11)	17.9350(7)
b (Å)	12.7010(7)	12.8340(17)	12.6580(4)	12.5580(5)	28.4340(15)
c (Å)	30.807(2)	30.446(3)	30.1260(4)	30.4720(18)	20.8150(10)
β (deg)	115.114(2)	116.390(3)	116.748(2)	114.322(2)	107.260(3)
V (Å^3)	10105.4(9)	9956.1(17)	9618.9(5)	10175.5(8)	10136.9(8)
Z	4			4	4
D_c (mg cm^{-3})	1.452	1.474	1.566	1.460	1.579
F(000)	4464		4592	4528	4868
μ (Mo Kα) (mm^{-1})	0.724	0.735	0.764	0.720	0.752
crystal size (mm)	0.04 × 0.04 × 0.08			0.02 × 0.04 × 0.04	0.02 × 0.02 × 0.06
total reflections	5514	5340	7018	4559	8629
reflections [$I > 2\sigma(I)$]	1427	1486	3062	2076	2851
R_1 [$I > 2\sigma(I)$][a]	0.1249	0.1516	0.0996	0.0636	0.0979
wR [$I > 2\sigma(I)$][a]	0.2966	0.3245	0.2141	0.1549	0.2641
S	0.967	1.017	1.052	0.836	1.018

[a] $R_1 = \sum||F_o| - |F_c||/\sum|F_o|$; $wR = \{\sum[w(F_o^2 - F_c^2)^2]/\sum w(F_o^2)^2\}^{1/2}$; $w = 1/[\sigma^2(F_o^2) + (mP)^2 + nP]$ where $P = (F_o^2 + 2F_c^2)/3$; $m = 0.2000$ (**1** (370 K)), 0.2000 (**1** (293 K)), 0.1142 (**1** (100 K)), 0.1432(**2**) and 0.1529 (**3**); $n = 0.0000$ (**1** (370 K)), 0.0000 (**1** (293 K)), 24.2433 (**1** (100 K)), 0.0000 (**2**) and 38.5177 (**3**).

No change of space group was observed during the desolvation process to give **1**. The only derived consequence of this transformation was the loss of quality of the crystal data.

1/1·CH$_3$CN·H$_2$O displays the monoclinic *C*2/*c* space group in the range of temperatures 100−370 K. The structure is made up of square-shaped tetranuclear cationic units characterized by a 2-fold axis running along [010] direction, which is perpendicular to the square's plane passing through the middle of the window. This 2-fold axis relates the two halves of the square by symmetry. Accordingly, the asymmetric unit is defined by two distinct iron(II) sites shown separately in Figure 1 for clarity. Table 2 gives representative bond lengths and distances for **1**.

The Fe(1) is surrounded by two phen bidentate ligands and two cyanide bridging groups in a *cis* position defining a slightly distorted octahedron with a [Fe(1)N$_4$C$_2$] coordination core. At 100 K the average Fe(1)−N(phen) bond distance is slightly larger than the Fe(1)−CN bond lengths, 1.971(9) Å and 1.908(13) Å, respectively. The angles around the Fe(1) site are close to 180° (in the range 175−177°) and 90°. The largest deviation from the right angle, determined by the geometry of the phen ligands, involve the angles N(1)−Fe(1)−N(2) = 82.5(4)° and N(3)−Fe(1)−N(4) = 82.4(4)°. The Fe(2) site is surrounded by a tetradentate TPMA ligand and two cyanide anions defining a slightly distorted octahedron with a [Fe(2)N$_6$] coordination core. The average Fe−N(TPMA) and Fe−NC bond distances are 1.966(9) Å and 1.942(10) Å, respectively. The angles of the [Fe(2)N$_6$] core are close to those expected for a regular octahedron. The largest deviations are found for N(7)−Fe(2)−N(10) [166.2(4)°], N(8)−Fe(2)−N(10) [82.9(4)°], and N(7)−Fe(2)−N(8) [83.4(4)°]. These bond distances and angles are characteristic of an iron(II) ion in the low-spin state.

The neutral complex [Fe(phen)$_2$(CN)$_2$] acts as a ligand through the N(5) and N(6) atoms of the cyanide groups, which are in a *cis* positions defining an angle close to 90° [C(25)−Fe(1)−C(26) = 91.3(4)°], a fact which favors the formation of the [Fe$_4$(μ-CN)$_4$(phen)$_4$(TPMA)$_2$)]$^{4+}$ tetranuclear square cationic species (Figure 2). The crystal packing of **1**, shown in Figure 3, could be dissected on chains of [Fe$_4$(μ-CN)$_4$(phen)$_4$(TPMA)$_2$)]$^{4+}$ units running along *x* and *z* direction. The phen ligands belonging to consecutive tetranuclear cations display $\pi\cdots\pi$ contacts shorter than the sum of the van der Waals radii [C(15)····C(23)^{i} = 3.49(2) Å, C(16)····C(23)^{i} = 3.64(2) Å, and C(18)····C(14) = 3.65(2) Å; i = (1/2 − *x*, 1/2 + *y*, 1/2 − *z*)]. There are additional C····C contacts between the TPMA ligands [C(34)····C(36)^{ii} = 3.51(2) Å, C(35)····C(35)^{ii} = 3.63(2) Å, C(35)····C(36)^{ii} = 3.55(2) Å, C(35)····C(37) = 3.63 (2) Å; ii = (−*x*, 1 − *y*, *z*)]. Furthermore, intra-square TPMA-phen short contacts are also present [C(29)····C(3)^{iii} = 3.46(3) Å, C(29)····C(4)^{iii} = 3.54(3) Å, C(29)····C(6)^{iii} = 3.64(3) Å, C(30)····C(4)^{iii} = 3.45(2) Å, and C(30)····C(6)^{iii} = 3.35(2) Å; iii = (−*x*, *y*, 1/2 − *z*)].

Each tetranuclear cation is surrounded by four PF_6^- anions. Furthermore, there is a water molecule and an acetonitrile molecule per tetranuclear cation at 100 K (see Figure 3). The PF_6^- anions and the water molecule do not display significant intermolecular interactions. In contrast, the acetonitrile molecule, which is inside of the pocket defined by phen, TPMA, and CN^- ligands (Figure 2), shows short C····C contacts with phen [C(45)····C(14)^{iii} = 3.66(2) Å, C(45)····C(13)^{iii} = 3.56(2) Å], TPMA [C(45)····C(44)^{iii} = 3.69(2) Å, C(46)····C(44)^{iii} = 3.48(2) Å], and CN^- [C(46)····C(26)^{iii} = 3.53(2) Å] (Figure 2).

At 293 K, the structural parameters change just slightly compared to the corresponding values at 100 K, the main difference being the complete loss of the acetonitrile and water molecules. At room temperature the Fe(2) site remains practically in the LS state, a fact which is in full agreement with the magnetic susceptibility at this temperature. Similarly, the crystallographic data at 370 K confirms the loss of the

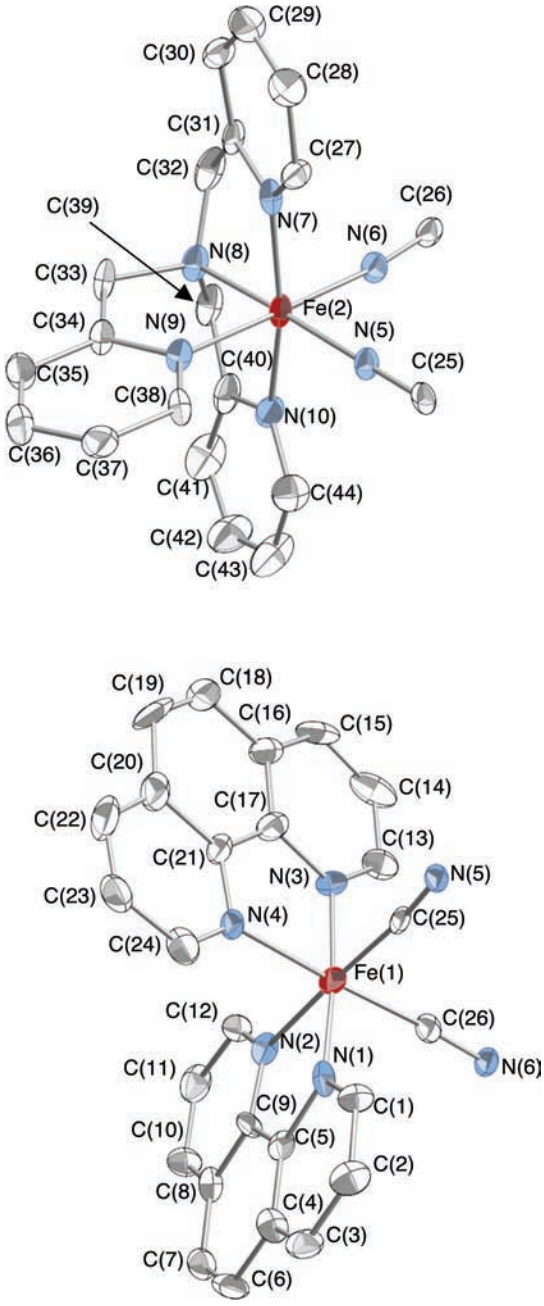

Figure 1. Oak Ridge Thermal Ellipsoid Plot (ORTEP) representations and atom numbering for the two molecular moieties involved in the tetranuclear $[Fe_4(\mu\text{-}CN)_4(phen)_4(TPMA)_2)]^{4+}$ cations. Hydrogen atoms have not been included for the sake of simplicity. Thermal ellipsoids are presented at 30% probability.

solvent molecules. Furthermore, there is unequivocal evidence of significant structural changes associated with the occurrence of a reversible LS-to-HS spin state change in the Fe(2) site. The average Fe(2)−N bond distance increases from 1.958(10) Å (100 K) up to 2.14(2) Å. Concomitantly with this fact, the N−Fe(2)−N angles display significant variations. The largest one corresponds to the N(7)−Fe(2)−N(10) angle which decreases by 11.4°. The angles N(5)−Fe(2)−N(7), N(5)−Fe(2)−N(6), N(6)−Fe(2)−N(9), N(5)−Fe(2)−N(8), N(7)−Fe(2)−N(8), N(9)−Fe(2)−N(8), N(9)−Fe(2)−N(10), N(8)−Fe(2)−N(10) show also important variations +6.3°, +5.8°, −5.6°, −7.2°, −6.3°, −8.1°, −5.5°, and −5°, respectively (the sign indicates the increase or decrease of each angle when moving from 370 to 100 K). The increase of the Fe(2)−N bond length agrees well with what is expected for an almost complete spin transition in iron(II) complexes. No significant variations were found for the Fe(1) site.

Table 2. Selected Bond Lengths [Å] and Angles [deg] for **1**, **2** and **3**

	1			**2**	**3**
	370 K	293 K	100 K	293 K	160 K
Fe(1)−N(1)	1.93(2)	1.93(2)	1.919(9)	1.970(9)	1.952(13)
Fe(1)−N(2)	2.01(2)	2.01(2)	2.003(9)	1.987(10)	1.985(13)
Fe(1)−N(3)	1.98(2)	1.96(2)	1.960(9)	1.974(9)	1.971(13)
Fe(1)−N(4)	2.05(2)	1.98(2)	2.001(9)	2.004(10)	2.020(12)
Fe(1)−C(25)	1.91(3)	1.87(3)	1.924(13)	1.920(15)	1.897(15)
Fe(1)−C(26)	1.92(3)	1.90(3)	1.893(11)	1.908(14)	1.918(17)
Fe(2)−N(5)	2.02(2)	1.99(2)	1.934(10)	2.042(10)	2.084(13)
Fe(2)−N(6)	2.07(2)	1.94(2)	1.950(9)	2.075(11)	2.092(14)
Fe(2)−N(7)	2.18(2)	1.96(2)	1.937(9)	2.260(11)	2.294(13)
Fe(2)−N(8)	2.18(2)	1.99(2)	1.979(9)	2.236(10)	2.219(11)
Fe(2)−N(9)	2.18(2)	1.96(2)	1.964(8)	2.209(12)	2.196(13)
Fe(2)−N(10)	2.20(2)	1.97(2)	1.985(9)	2.224(12)	2.347(12)
N(1)−Fe(1)−N(2)	85.3(8)	84.1(9)	82.5(4)	82.2(5)	82.7(6)
N(1)−Fe(1)−N(3)	175.1(8)	175.4(9)	175.2(4)	174.4(5)	173.4(5)
N(1)−Fe(1)−N(4)	93.8(8)	94.0(9)	94.3(4)	94.6(5)	92.3(5)
N(1)−Fe(1)−C(25)	92.9(9)	93.1(10)	93.5(4)	94.1(5)	96.1(6)
N(1)−Fe(1)−C(26)	90.3(8)	86.1(9)	87.9(4)	89.1(4)	89.8(5)
N(2)−Fe(1)−N(3)	91.1(8)	92.2(8)	94.2(4)	93.3(4)	94.0(5)
N(2)−Fe(1)−N(4)	90.8(7)	91.2(8)	93.4(3)	91.9(4)	91.9(5)
N(2)−Fe(1)−C(25)	177.7(9)	176.5(9)	176.0(4)	176.2(5)	178.8(6)
N(2)−Fe(1)−C(26)	88.2(8)	87.9(9)	88.1(4)	88.7(4)	89.4(5)
N(3)−Fe(1)−N(4)	82.9(9)	83.4(9)	82.4(4)	82.2(5)	82.1(5)
N(3)−Fe(1)−C(25)	90.6(9)	90.5(9)	89.8(4)	90.4(4)	87.2(6)
N(3)−Fe(1)−C(26)	93.0(9)	96.5(9)	95.4(4)	94.1(5)	95.9(5)
N(4)−Fe(1)−C(25)	88.0(9)	86.9(9)	87.4(4)	89.5(4)	88.1(5)
N(4)−Fe(1)−C(26)	175.8(9)	179.1(10)	177.5(4)	176.3(5)	177.6(6)
C(25)−Fe(1)−C(26)	93.2(10)	94.0(10)	91.3(4)	90.2(5)	90.6(6)
N(5)−Fe(2)−N(6)	94.6(8)	90.2(7)	88.8(3)	94.6(4)	91.0(5)
N(5)−Fe(2)−N(7)	104.7(9)	99.7(8)	98.4(4)	116.4(5)	109.9(5)
N(5)−Fe(2)−N(8)	170.9(9)	176.8(8)	178.1(4)	166.4(4)	176.3(5)
N(5)−Fe(2)−N(9)	93.0(8)	92.3(8)	93.3(4)	91.8(5)	99.9(5)
N(5)−Fe(2)−N(10)	99.6(9)	94.8(9)	95.4(4)	92.8(5)	101.8(4)
N(6)−Fe(2)−N(7)	90.3(8)	87.9(9)	89.0(3)	86.5(4)	88.7(5)
N(6)−Fe(2)−N(8)	94.3(9)	92.5(8)	91.8(4)	95.2(4)	91.2(4)
N(6)−Fe(2)−N(9)	172.3(9)	177.0(8)	177.9(4)	173.6(5)	169.1(5)
N(6)−Fe(2)−N(10)	94.7(9)	93.8(8)	91.0(4)	97.7(4)	98.3(5)
N(7)−Fe(2)−N(8)	77.1(9)	82.1(8)	83.4(4)	73.7(5)	73.3(5)
N(7)−Fe(2)−N(9)	89.0(9)	89.9(7)	91.1(3)	90.1(4)	86.5(4)
N(7)−Fe(2)−N(10)	154.8(9)	165.3(10)	166.2(4)	150.2(5)	147.4(4)
N(8)−Fe(2)−N(9)	78.0(9)	85.1(8)	86.1(4)	78.6(5)	78.1(5)
N(8)−Fe(2)−N(10)	77.9(9)	83.3(9)	82.9(4)	76.5(5)	74.8(5)
N(9)−Fe(2)−N(10)	82.8(10)	87.7(8)	88.3(4)	82.5(4)	80.7(4)

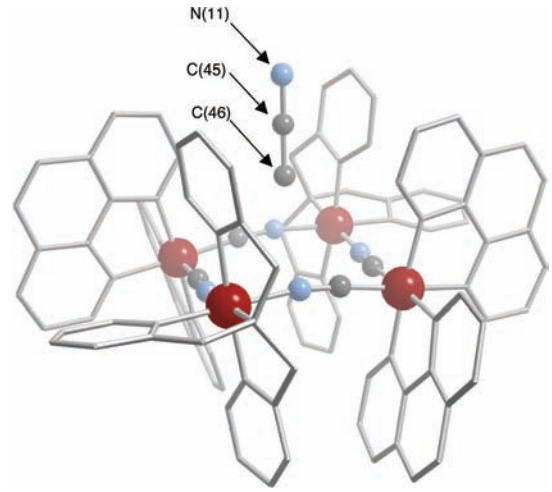

Figure 2. Representation of a $[Fe_4(\mu\text{-}CN)_4(phen)_4(TPMA)_2)]^{4+}$ square illustrating the pocket generated by the phen and TPMA ligands where the acetonitrile molecule is placed.

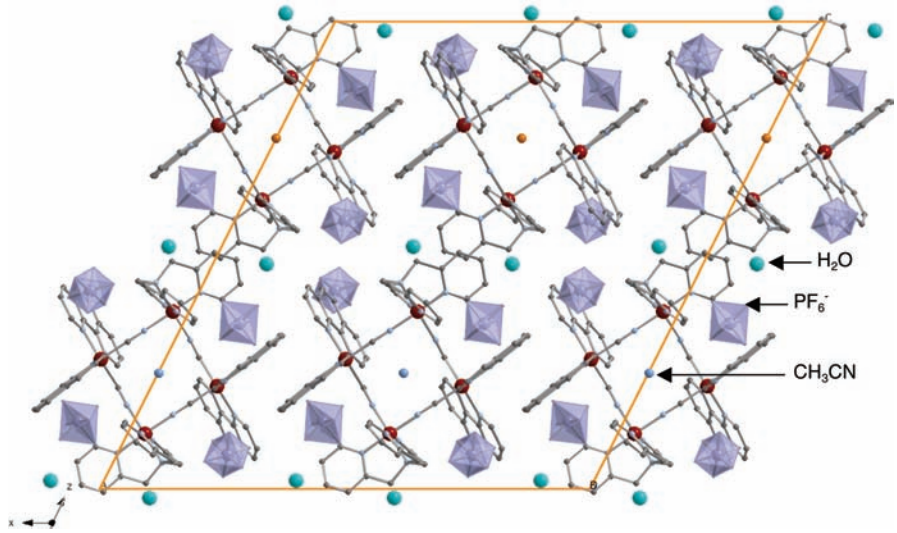

Figure 3. Crystal packing of $[Fe_4(\mu\text{-}CN)_4(phen)_4(TPMA)_2)](PF_6)_4 \cdot [CH_3CN,H_2O]$ (T = 100 K).

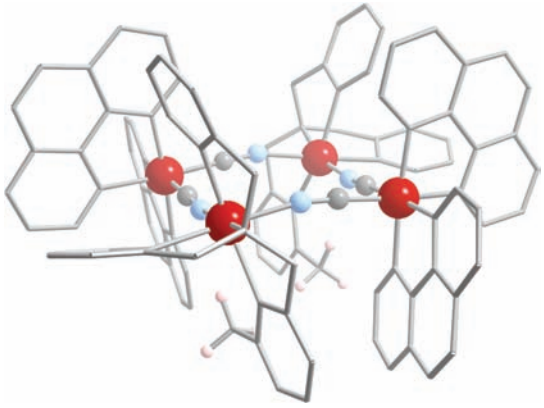

Figure 4. Schematic view of $[Fe_4(\mu\text{-}CN)_4(phen)_4(MeTPMA)_2)]^{4+}$ cation.

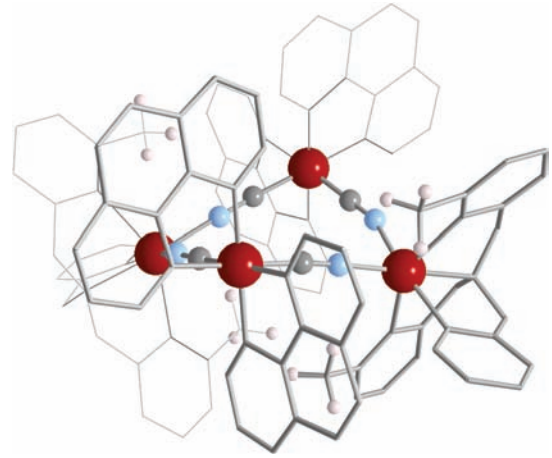

Figure 5. Schematic view of $[Fe_4(\mu\text{-}CN)_4(phen)_4(Me_2TPMA)_2)]^{4+}$ cation.

The intermolecular distances increase somewhat, although some of them still remain smaller than the sum of the van der Waals radii, namely C(15)····C(23)^{i} = 3.64(4) Å, C(29)····C(4)^{iii} = 3.61(6) Å, C(29)····C(6)^{iii} = 3.64(3) Å, C(30)····C(4)^{iii} = 3.45(2) Å and C(30)····C(6)^{iii} = 3.41(6) Å.

Crystal Structure of 2. Compound **2** crystallizes in the monoclinic *C*2/*c* space group displaying a structure quite similar to that described for **1** at 293 K (see Table 1). The atom numbering for both moieties $[Fe(phen)_2(CN)_2]$ and $[Fe(MeTPMA)(NC)_2]$ have been kept the same as for **1**. Significant bond distances and angles are shown in Table 2. The $[Fe(phen)_2(CN)_2]$ moiety is, within the error limits, practically identical to that of **1**, the average bond length for the $[Fe(1)N_4C_2]$ core being 1.961(15) Å. The main differences are observed in the $[Fe(MeTPMA)(NC)_2]$ moiety where the methyl group induces steric hindrance in the $[FeN_6]$ core thus diminishing the ligand field strength and stabilizing the HS state of the Fe(2) site (see Figure 4). This is clearly illustrated by the Fe(2)−N(7) = 2.260(11) Å, Fe(2)−N(8) = 2.236(10) Å, Fe(2)−N(9) = 2.209(12) Å, Fe(2)−N(10) = 2.224(12) Å bond lengths, which are on average 0.26 Å larger than in **1** at 293 K whereas Fe(2)−N(5) = 2.042(10) Å and Fe(2)−N(6) = 2.075(11) Å increase about 0.09 Å on average. In particular, the Fe(2)−N(7) bond, where the nitrogen atom belongs to the methyl substituted pyridine ring, is 0.30 Å longer than in **1**. The steric hindrance is also clearly reflected in the angle N(5)−Fe(2)−N(7) = 116.4(5)° which is 16.7° (11.7°) larger than in **1** at 293 K (370 K). The crystal packing is essentially the same as for **1** (see Supporting Information); however, the tetranuclear cations are more separated from each other in **2**. In fact, it is only possible to account for two C(phen)····C(phen) contacts [C(24)····C(18)^{i} = 3.58(2) Å and C(23)····C(16)^{i} = 3.68(2) Å] and one C(phen)-CH_3 contact [C(23)····C(15) = 3.69(2) Å], which is directed along the *y* axis ($i = -x + 1/2, y - 1/2, -z + 1/2$).

Crystal Structure of 3. Compound **3** crystallizes, like **1** and **2**, in the monoclinic *C*2/*c* space group. In spite of this, the crystal parameters and the crystal packing are quite different. The molecular structure of **3** is displayed in Figure 5. Selected bond distances and angles are shown in Table 2 (atom numbering remains the same as for **1** and **2**). The Fe(1) site, which corresponds to the LS $[Fe(phen)_2(CN)_2]$ moiety, has Fe−N distances and angles comparable to those observed for **1** and **2**. Concerning site Fe(2), the $[FeN_6]$ octahedron is more distorted than in **2**, for example the axial bonds Fe(2)−N(10) and Fe(2)−N(7) are affected by the presence

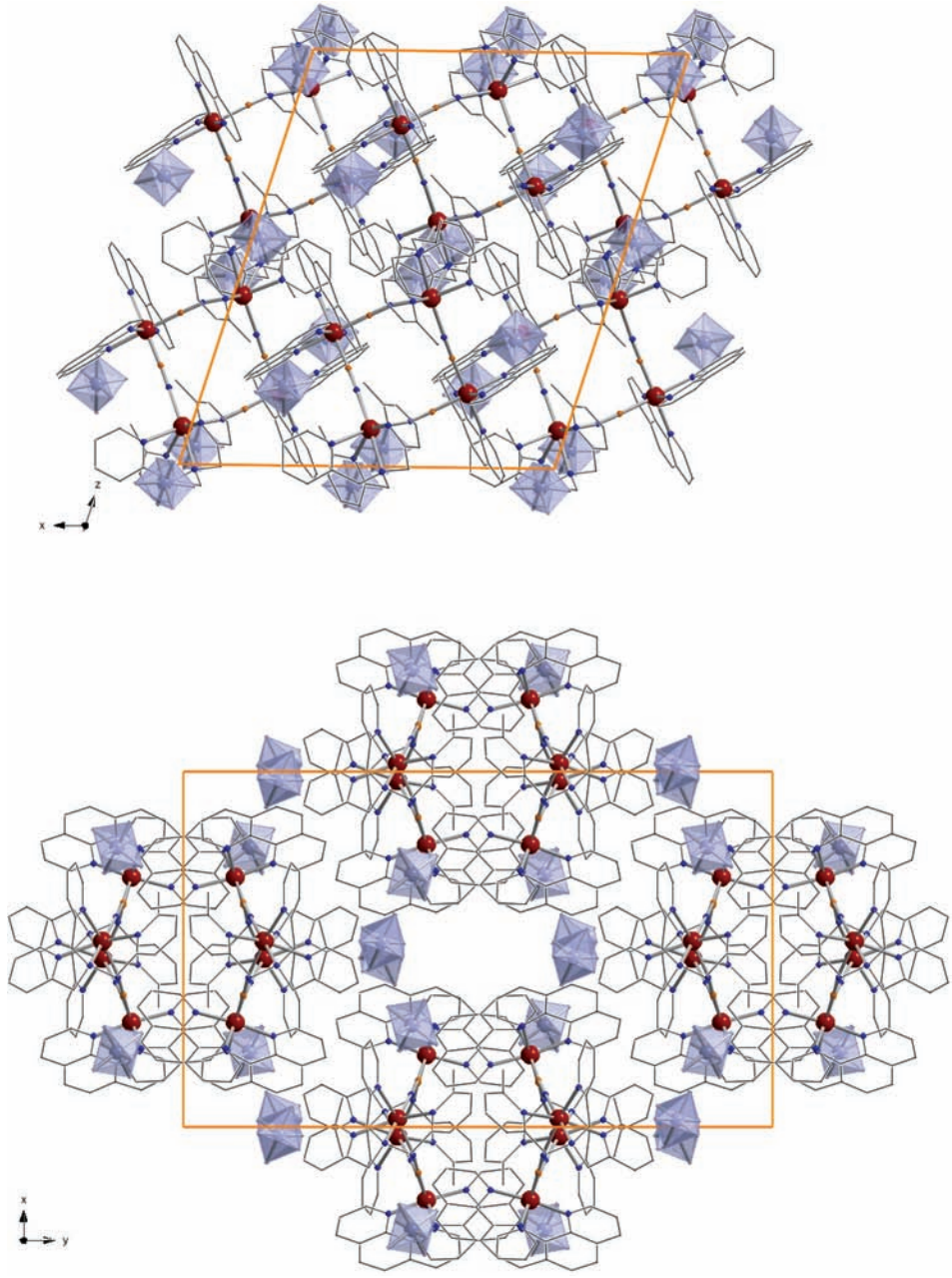

Figure 6. Top: Projection of the unit cell of **3** on the *xz* plane ([010] direction) showing the relative disposition of the squares and PF_6^- anions. Bottom: Projection of the unit cell of **3** along [001] direction showing a large channel in the center of the unit cell.

of the two methyl groups [C(45) and C(46)] attached to the atoms C(27) and C(44) of their respective pyridine rings. The Fe(2)−N(10) and Fe(2)−N(7) bonds are 0.123 and 0.034 Å longer than observed for **2**. Furthermore, the angle N(7)−Fe(2)−N(10) decreases by 2.8°. These structural modifications allow the N(8) to approach the Fe(II) ion, making shorter the Fe(2)−N(8) distance by 0.017 Å. In addition, the angle N(5)−Fe(2)−N(7) becomes 6.5° smaller while the angles N(5)−Fe(2)−N(8), N(5)−Fe(2)−N(9), and N(5)−Fe(2)−N(10) are 9.9°, 8.1°, and 9.0° larger, respectively, in comparison with **2**. This local distortion leads to the folding of the $[Fe]_4$ square through its diagonal defining an angle between the two triangular halves of 136°.

The crystal packing seen along the [010] direction is similar to that shown in Figure 3 for **1**. The whole packing could be described as formed by chains of tetranuclear cations running parallel to the [001] direction, while the chains stack along [100]; the resulting sheets lying in the *xz* plane propagate along the [010] direction (Figure 6a). Within a chain, the 6-methylpyridine moieties and phenanthroline ligands interdigitate in such a way that the former is placed between a phenanthroline ligand and a 6-methylpyridine of an adjacent tetranuclear cation (see Supporting Information, Figure S2) giving two types of short intermolecular π-π interactions pointing to [100] direction. One is defined by the interaction of the two 6-methylpyridine moieties belonging to two tetranuclear species [C(42)····C(44)^i = 3.38(3) Å, C(41)····C(43)^i = 3.58(3) Å, C(40)····C(43)^i = 3.42(2) Å and C(41)····C(44)^i = 3.45(3) Å], while the other one is defined by a 6-methylpyridine and a phenanthroline molecule

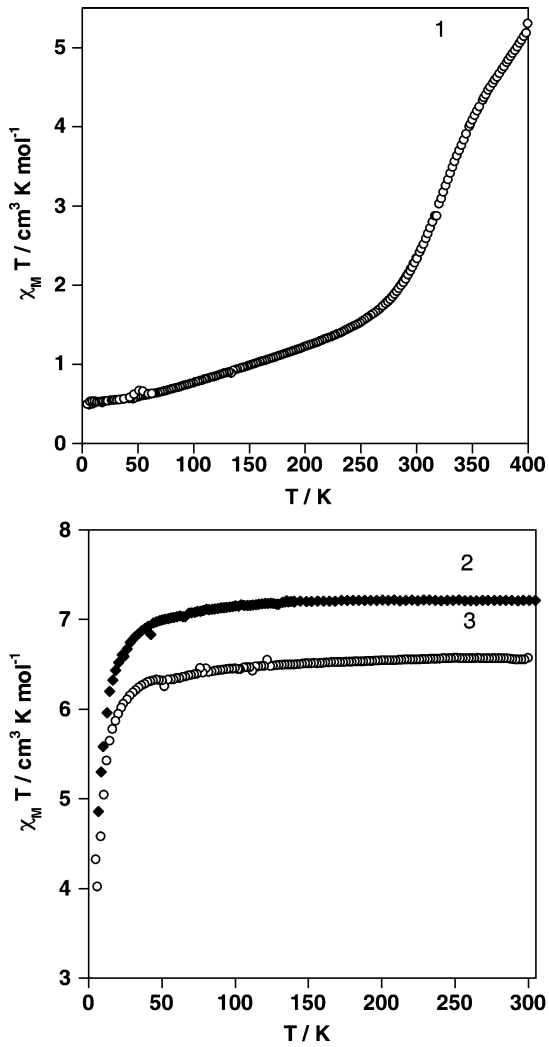

Figure 7. $\chi_M T$ versus T plots for compounds **1** (top), **2**, and **3** (bottom).

[C(4)$\cdots$C(43)^i = 3.45(3) Å, C(5)$\cdots$C(43)^i = 3.51(3) Å, C(4)$\cdots$C(42) = 3.556 Å] ($i = -x + 1, -y, -z$).

Along [001] direction the organization of the tetranuclear cations define large channels centered in the middle and the four corners of the unit cell. Although these channels are partially occupied by the PF_6^- anions, the accessible solvent volume calculated using Platon indicates that there are two voids of 503 Å^3 each one,[16] which represent 10% of the total volume of the unit cell. Within the voids, there is a non-assigned electronic density perfectly compatible with the occurrence of two NH_4^+ cations per void with an occupancy factor of 0.5. Although it has not been possible to identify directly the NH_4^+ group, this assignment is based on the following experimental facts: (i) the use of an excess of NH_4PF_6 in the synthetic procedure, (ii) the presence of five PF_6^- anions per tetranuclear cation, and (iii) the occurrence of four divalent iron ions according to the Mössbauer spectrum (see Supporting Information, Figure S3).

Magnetic Properties. The magnetic behavior of **1** expressed as the product $\chi_M T$ vs T, where χ_M is the magnetic susceptibility and T the temperature, is shown in Figure 7. At 400 K, $\chi_M T$ is equal to 5.3 cm^3 K mol^{-1} and decreases continuously with temperature to reach a value of 1.7 cm^3 K mol^{-1} at 264 K. Then, $\chi_M T$ decreases less markedly down to 0.5 cm^3 K mol^{-1} at 4 K. Below 50 K it is safe to state that the four irons are fully in the LS state. Given the poor cooperativity of the spin conversion, warming-cooling cycles take place without hysteresis.

At 400 K, the $\chi_M T$ value per tetranuclear cation is smaller than expected for two Fe(II) in the HS state (ca. 6−7.6 cm^3 K mol^{-1}) indicating that about 12−30% of the SCO centers are still in the LS state at this temperature. Taking into account the structural data of **1**, the Fe(1) sites are in the LS spin state in the whole range of temperatures investigated while the Fe(2) sites are SCO centers.

Compounds **2** and **3** have similar magnetic behaviors (Figure 7). $\chi_M T$ is equal to 7.2 and 6.6 cm^3 K mol^{-1} at 300 K, for **2** and **3**, respectively. These correspond to the expected values for two iron(II) ions [Fe(2) site] in the HS state. As temperature decreases, $\chi_M T$ decreases smoothly down to about 6.9 cm^3 K mol^{-1} (**2**) and 6.3 cm^3 K mol^{-1} (**3**) at 40 K, then decreases more rapidly to reach a value of 4.8 cm^3 K mol^{-1} (**2**) and 4.0 cm^3 K mol^{-1} (**3**) at 5 K. This behavior is reminiscent of occurrence of zero-field splitting of the local $S = 2$ ground spin state; however, very weak antiferromagnetic interactions mediated by the [Fe(1)(phen)$_2$(CN)$_2$] diamagnetic moieties cannot be entirely excluded.

Discussion

This work was undertaken aiming at investigating the SCO phenomenon in new square shaped iron(II) tetranuclear molecules. It was motivated by previous work done by Vahrenkamp, Oshio, and co-workers who synthesized the square complexes [Fe$_4$(μ-CN)$_4$(2,2′-bipy)$_4$(TPMA)$_2$](X)$_4$ (X = PF_6^- or BF_4^-). In the BF_4^- salt, the [Fe$_4$(μ-CN)$_4$(2,2′-bipy)$_4$(TPMA)$_2$]$^{4+}$ cation has the same symmetry as its phen homologous counterpart in **1**. In fact, both compounds crystallize in the same space group. In contrast, the PF_6^- salt of the bipy derivative is less symmetric and displays four crystallographically different iron(II) sites, all of them in the LS state at 100 K. Oshio and co-workers have demonstrated that the Fe(TPMA) sites undergo a reversible two-step spin transition characterized by two well separated characteristic temperatures. A first step takes place in the temperature range 100−210 K while the second step starts at about 300 K and finishes at temperatures higher than 400 K. Between both steps there is a large plateau, about 100 K wide, where a Fe(TPMA) site is in the HS, and the other remains in the LS state. This behavior is reminiscent of that previously reported for the dinuclear complex {[Fe(bztpen)]$_2$[N(CN)$_2$]}(PF$_6$)$_3$. In the latter compound, only one iron(II) site was observed at all measured temperatures, even in the middle of the plateau where, probably, an averaged intermediate LS-HS state exists. In this compound, a transition between dynamic and static disorder of the dicyanamide bridging ligand was found correlated with the two-step nature of the transition.[17]

(16) Spek, A. L. *J. Appl. Crystallogr.* **2003**, *36*, 7.

(17) Ortega-Villar, N.; Thompson, A. L.; Muñoz, M. C.; Ugalde-Saldívar, V. M.; Goeta, A. E.; Moreno-Esparza, R.; Real, J. A. *Chem.—Eur. J.* **2005**, *11*, 1.

A priori, this square "design" strategy for constructing tetranuclear SCO molecules is quite promising since these species may be rationally synthesized by assembling a variety of suitable molecular building blocks and thus fine-tune the nature of the SCO behavior. In this regard, we wanted to study the modification of the SCO properties of the tetranuclear species when the 2,2′-bipy ligand is replaced by the phen ligand, on one hand, and the effects of the steric hindrance generated by a methyl group attached to the sixth position of one or two 2-pyridylmethyl moieties of the TPMA ligand, on the other hand.

Microcrystalline solids of **1**−**3** where prepared via diethyl ether vapor diffusion in CH_3CN solutions of the corresponding solids previously precipitated in methanol by addition, in all cases, of a NH_4PF_6 excess for facilitating the crystal growth. However, observation of rapid deterioration of the single crystals of "**1**", indicating possible loss of solvent, prompted us to select a single crystal from the mother liquor and immediately to freeze it at 100 K to get reasonably good X-ray diffraction data. At this temperature "**1**" shows the presence of a molecule of H_2O and one of CH_3CN. Hence, the real formula is **1·CH$_3$CN·H$_2$O**. However, at ambient conditions **1·CH$_3$CN·H$_2$O** rapidly transforms into **1**, which is the stable form for this compound, a fact consistent with the corresponding chemical analysis of the microcrystalline powder and correspondence of the XRPD patterns to the simulated ones of the microcrystalline powder (see Supporting Information, Figure S4).

A consequence of the steric effects induced by the methyl groups seems to be the bent conformation adopted by the tetranuclear species in **3**, a fact that changes significantly the crystal packing. It is characterized by the formation of large channels essentially filled with NH_4^+ cations coming from the inclusion of an ion pair $(NH_4^+)(PF_6^-)$ per tetranuclear cation.

The magnetic behavior of **1** denotes the occurrence of a gradual poor cooperative spin transition, which takes place in the temperature range 100−400 K. At 400 K both phen and 2,2′-bipy derivatives reach similar LS-to-HS conversion levels since $\chi_M T$ is about 5−5.4 cm^3 K mol^{-1} for both compounds at 400 K. The most relevant difference is the two-step character of the 2,2′-bipy derivative with the low temperature step being relatively steep. Usually, two-step spin-state conversion occurs in the solid state when singular correlations between intra- and intermolecular interactions are met. In this respect, 2,2′-bipy and phen derivatives display different crystal packing. The former crystallizes in the triclinic $P\bar{1}$ space group with the square motifs lacking of molecular symmetry. In contrast, the latter crystallizes in the monoclinic $C2/c$ space group, and a 2-fold axis passes perpendicular to the plane of the square motif through its barycenter. Consequently, the squares derived from **1** are more symmetric than those of the 2,2′-bipy compound. For example, the relative orientation of the TPMA ligands, in particular the almost linear N(amino)(TPMA)-Fe−NC-Fe-(bipy)$_2$ motifs, define an angle of about 90° in the 2,2′-bipy derivative while these fragments are parallel to each other in **1**; hence, the organization of the squares in the crystal is different for both compounds. Furthermore, the [Fe$_4$] square unit is more distorted in the 2,2′-bipy compound, the Fe atoms deviate from the mean plane [Fe$_4$] by 0.25−0.26 Å, in addition two N atoms belonging to the CN groups, which define two edges of the square, are at 0.645 [N(2)] and 0.337 [N(1)] Å from this plane. At 293 K the Fe(1) and Fe(2) atoms separate 0.157 Å from the [Fe$_4$] plane, and this separation vanishes at 370 K in **1**. The average Fe−N bond distances at 300 K of the LS-[Fe(TPMA)(NC)$_2$] fragment in the 2,2′-bipy compound and those in **1** at 293 K are virtually identical (1.967 Å) indicating that the ligand field strength in this fragment of the 2,2′-bipy compound is identical to the ligand field in the two SCO irons in **1**. Indeed, the incomplete high temperature step of the 2,2′-bipy compound and the spin conversion of **1** take place in the same temperature interval. However, the other [Fe(TPMA)(NC)$_2$] fragment of the 2,2′-bipy compound is HS at 300 K indicating that it is in a weaker ligand field. Inspection of the crystal packing of the 2,2′-bipy derivative shows that there are strong discrete π-π interactions between two pyridine rings of two consecutive squares (C···C in the range 3.404−3.581 Å). These interactions have also been described for **1**; however, they are less intense and, as a consequence of symmetry, occur in the two [Fe(TPMA)(NC)$_2$] fragments generating an infinite chain which extends parallel to z (see Figure 3). Contrarily to **1**, these π-π interactions only occur in one [Fe(TPMA)(NC)$_2$] fragment of the 2,2′-bipy derivative while the other does not show any remarkable short intermolecular contact. This difference between the two [Fe(TPMA)(NC)$_2$] sites could be the cause of the two-step character of the SCO in 2,2′-bipy derivative. Indeed, the π-π interactions occur between aromatic rings directly involved in the coordination sphere of the SCO iron, and this could affect somehow the ligand field strength of the involved iron atoms. Thus, in the framework of this discussion, the observation of only one simultaneous SCO is consistent with the equivalence of the two [Fe(TPMA)(NC)$_2$] in **1**. However, these sensible conjectures do not explain why the iron sites involved in the π-π interactions in both compounds display spin state conversions separated more than 100 K. A possible cause of this could be the different chemical pressure supported by the squares in both compounds. It is worth noting that such subtle solid-state singularities may provoke drastic responses in a SCO system.[18]

The magnetic behavior of compounds **2** and **3** corresponds to that expected for HS iron(II) compounds. The lack of SCO is a consequence of the steric hindrance and accordingly of the lowered ligand field strength generated by the methyl groups attached to the 6th position of the pyridin-2-ylmethyl moiety of the TPMA ligand.[19] The average Fe(2)−N bond distances are R = 2.14, 2.17, and 2.20 Å for **1** (370 K), **2**, and **3**, respectively. The regular increment of these distances is accompanied by a decrease of the ligand field strength

(18) See for example: (a) Dupouy, G.; Marchivie, M.; Triki, S.; Sala-Pala, J,; Salaün, Y. Y.; Gómez-García, C. J.; Guionneau, P. *Inorg. Chem.* **2008**, *47*, 8921. (b) Moliner, N.; Muñoz, M. C.; Létard, S.; Létard, J. F.; Solans, X.; Burriel, R.; Castro, M.; Kahn, O.; Real, J. A. *Inorg. Chim. Acta* **1999**, *291*, 279.

(19) Goodwin, H. A. *Top. Curr. Chem.* **2004**, *233*, 59.

10Dq, which is proportional to $1/R^6$. In fact a decrease of 10Dq of about 10% and 20% can be estimated when moving from **1** (370 K) to **2** and **3**, respectively.

Conclusion

The investigation of three $[Fe_4(\mu\text{-}CN)_4(phen)_4(L)_2)](PF_6)_4$ "square" type complexes with TPMA (tris(pyridin-2-ylmethyl)amine) type ligands has demonstrated that a minor change from the 2,2′-bipy of the prototypal analogue to phen eliminates the two step SCO in favor of one step. The probable reason is the higher symmetry of the $[Fe_4(\mu\text{-}CN)_4(phen)_4(TPMA)_2)](PF_6)_4$ in solid state and the disturbed balance between inter- and intramolecular forces causing the destabilization of the HS-LS plateau and hence no observation of a two-step transition. The use of methylated TPMA analogues proved to impose too much hindrance and consequently suppression of the SCO behavior. The results reported here manifest the importance of weak balance between different factors for determining the SCO properties in this class of compounds.

Acknowledgment. Financial support is acknowledged from the Spanish Ministerio de Educación y Ciencia (MEC) (CTQ 2007-64727-FEDER) and from the European Network of excellence MAGMANET (Contract: NMP3-CT-2005-515767-2). A.B.G. thanks the Spanish MEC for a research contract (Programa Ramón y Cajal).

Supporting Information Available: Figures of the crystal packing of compound **2** (Figure S1) and interdigitation of 6-methylpyridine and phen ligands of different square cations in **3** (Figure S3), Mössbauer spectrum of **3** (Figure S3), experimental and calculated X-ray powder diffraction patterns of **1**, and CIF files of **1** (100, 293, and 370 K), **2** (293 K) and **3** (160 K). This material is available free of charge via the Internet at http://pubs.acs.org.

IC802306R